Supporting Information

Peñalver et al. 10.1073/pnas.1120499109

SI Text

Historical Context of Gymnosperm–Thrips Pollination. Plant–insect pollination mutualisms in certain cycad species consist of faithful pollination by specialist thrips pollinators that consume host-plant items such as pollen and tissues. Interactive insect behaviors in this process often are mediated by chemical and physical cues, such as volatile chemical emissions (1, 2) and cone thermogenesis (3), that serve in luring insects to their host plants. Such insect-mediated pollination is more efficient than wind pollination (4), and these pollinator mutualisms could be ancient for some taxa (5–7), extending into the preangiospermous Mesozoic. The greater efficiency of insect over wind pollination recently has been supported by the most basal and geochronologically earliest clade of cycads, the Cycadaceae, possessing various clades of beetle pollinators (1, 8–12), as well as pollen laden coprolites occurring in Middle Triassic male cones of a related taxon (13). Additionally, there are mid-Mesozoic and earlier Permian occurrences of prepollen and pollen feeding of seed plants by suspect Coleoptera and Thysanoptera (9, 14). As in modern cycads, the fossil record indicates that extinct seed-plant lineages previously considered fundamentally wind-pollinated also included taxa that display evidence consistent with insect pollination (15, 16). The fossil evidence in support of mid-Mesozoic seed-plant–insect associations and likely pollination has included insect mouthpart structure (16, 17), partly consumed ovulate and pollen organs and associated tissues (13, 15), ovulate organ structure (15, 16), external pollen features (18, 19), pollen associated with heads and mouthparts of suspect insects (15, 20), and the extant biologies of relevant insects and their gymnospermous hosts (9, 21–23). The current gymnosperm–thrips association adds to this repertoire of associations and represents an additional instance of such an interaction from amber.

Synchrotron Imaging Procedure. The holotype specimen of *Gymnopollisthrips minor* gen. et sp. nov. (Fig. 1 *B* and *C*) was imaged at the BM05 beamline of the European Synchrotron Radiation Facility at Grenoble, France, using propagation phase-contrast X-ray synchrotron microtomography. This technique reveals structural detail on samples lacking sufficient contrast for X-ray absorption techniques (24–26). To facilitate the 3D processing of the data, an algorithm for single-distance phase retrieval developed by Paganin et al. (27) was implemented. The algorithm developed by Paganin et al. already has been successfully applied for imaging on fossils (28) but, in the present case, was modified because the sample to image profile did not fit conditions for the application of such an algorithm.

The sample consisted of an amber piece embedded in epoxy resin and glued on a cover glass. The geometry of the sample clearly was not adapted for a single-phase retrieval process because of very strong absorption anisotropy during sample rotation. Because the insect structures were principally small in size, all structures larger than 50 pixels were removed, subtracting to each projection a copy of itself after a median filtering of 50 pixels. This operation of subtraction led to complete normalization of the background and optimization of the contrast of the insect itself, using the Paganin phase retrieval. To compensate for the blurring induced by the phase retrieval, a less-than-sharp mask filter was applied on the radiographs after the phase retrieval. Residual ring artifacts were corrected on the reconstructed slices and the volume was converted into a 16-bit tagged image file format (TIFF) stack file. The 3D images were manually rendered into a movie using a region-growing technique with VGStudiomax (version 2.1) software (Volume Graphics).

The scan was performed using a propagation distance of 24 mm and beam energy of 20 keV, implemented by a double-crystal multilayer monochromator. The movie consisted of 1,500 projections, each of which was acquired every 0.8 s over 180 degrees. To obtain a sufficiently high resolution of the fine structures in the specimen, a detector giving an isotropic voxel size of 0.75 μm was used.

The scanned amber piece was translucent (Fig. 2*I*) and potentially of high scientific value; consequently, it would have been risky to perform an elevated high-resolution scan. The equipment setup and protocol mentioned above typically are used for high-resolution scanning of opaque amber pieces (25, 27, 29). In the case of nonopaque amber, it is common to observe strong darkening of the amber during synchrotron imaging. Although the darkening can later be removed using UV light exposure, it always is preferable to avoid the potentially damaging effects of amber darkening and to reduce the dosage to an acceptable minimum level whenever possible, especially when dealing with potential holotype material. Accordingly, a high-efficiency and high-resolution detector was developed that would reduce the X-ray dose by nearly a factor of 50. This lower dose, compared with the much more elevated standard, produces a comparable dynamic level in the data but requires scanning times of approximately 1 h rather than a few minutes. As a consequence of a dramatic reduction in total X-ray flux, and the scanning time limited by the speed of the detector instead of the X-ray flux, it appeared more reasonable to use the beam of a bending magnet (BM05), instead of the far higher flux of an undulator, such as the ID19 beamline (28, 29).

The detector apparatus consisted of a single optical element from a 20× microscope objective with a 0.4-mm opening that was coupled with a 9 μm lutetium oxyorthosilicate (LSO) scintillator (29). The light was projected on a CCD FreLoN camera (30) containing a new-generation CCD chip (E2V) with a 15-μm pixel size, yielding five times greater efficiency than the Atmel chip generally used for these type of experiments. The combination of the LSO scintillator and a E2V FreLoN camera also allowed higher efficiency, attributable to scintillator emission as green light (550-nm emission ray), complimenting the maximum efficiency of the E2V CCD chip, compared with the red light (715 nm) of the usually used $Gd_3Ga_5O_{12}$ (GGG) scintillators. The principal drawbacks of this type of detector are: (*i*) a notably slow readout time of 0.6 s per frame; (*ii*) distortion attributable to the optical configuration that is corrected by retrodistortion of the pictures; and (*iii*) a loss of about 200 pixels on the total field of view compared with an optical system using both a 10× objective and a 2× eyepiece. Considering that the dose reduction and the longer scans did not result in darkening of the amber piece and the resulting data quality was similar to the alternative rapid and high-dose setup, this modified system was preferable for scanning by avoiding specimen damage. Because of adjustments to scan duration and dose intensity, some pollen grains were not detected by our procedure and, thus, not imaged in the resulting movie.

Geological Context. The Basque–Cantabrian Basin (BCB), northern Spain, along with other Mesozoic basins of the Iberian Peninsula, is associated with the opening of the northern part of the Atlantic. During the Early Cretaceous, sedimentation of the basin was dominated by sandstones, limestones, and marls that

were deposited in shallow marine and freshwater environments. During the lower–middle Albian, at the end of the rift stage, deltaic and estuarine systems developed and evolved vertically into a deltaic system dominated by a fluvial–deltaic environment with siliciclastic input, represented by the Escucha Formation (31). In general, the amber localities of the BCB are related to paralic environments in the eastern region (Escucha Fm.), or paralic–marine environments in the western region (Las Peñosas Fm.) (32). Spanish Cretaceous amber is principally found in localities distributed in a curvilinear arc from the east to the north along the Iberian Peninsula, which corresponds approximately to the seashore during the Early Cretaceous (33).

Two main amber-bearing outcrops are found in the eastern area of BCB: Moraza, also named Peñacerrada I in Burgos Province and Peñacerrada II (32) in Álava Province. The amber from both deposits is known as Álava amber (32). The palynological record suggests an Albian age (Early Cretaceous, *ca.* 110–105 Ma) for associated Álava amber. In this area, the Escucha Fm. is divided into three subunits that, overall, are represented by a deltaic succession, with a vertical tendency to a regression of the deltaic system in the lower–middle subunits and a vertical transgression in the upper subunit (31). The lower subunit is characterized by gray clays or heterolithic deposits with sparse intercalations of carbonate sandstones with orbitolinids. The middle subunit is dominated by sandstones and siliceous microconglomerates from channel fill and abundant coal beds. The upper subunit consists of gray lutites with intercalations of carbonate sandstones containing marine orbitolinids and bivalves. Amber is always associated with coal and lignitic beds or organically rich marl levels of the middle subunit, coinciding with the boundary between the maximum regression and the beginning of the transgression. Amber-bearing strata typically are located within sedimentary deposits of the interdistributary deltaic bays. One of these amber deposits occurs in Peñacerrada I amber, which has yielded the present thrips specimens and thousands of other arthropod inclusions (32–34).

Systematic Paleontology. ***Plants. Plant host affinities of the pollen.*** All pollen grains adhering to the thrips bodies have the same shape, minute size [average, 20.4 μm long (range, 17.4–24.9) and 12.6 μm wide (range, 9.3–15.4)] and sulcus and surface features and, consequently, are assignable to the same pollen form genus. The exine is 1.3 μm thick (range, 0.7–2.5 μm); some grains show weak exines that could be incompletely developed, aborted grains. Clusters of pollen grains occur principally in the holotype of *G. maior* sp. nov., despite their occasional detachment from thrips bodies that evidently occurred during initial resin immersion. These relationships indicate a physical or chemical basis for intergrain adhesion.

The pollen morphology (Figs. 1 *I* and *J* and 2*C*) corresponds to the gymnosperm form genus *Cycadopites* Wodehouse emend Fensome (35). This genus is based on material described from the Paleocene near Red Lodge, in Carbon County, southwestern Montana (36, 37). In particular, the pollen grains are favorably compared with Jurassic and Cretaceous specimens attributed to *C. follicularis* Wilson and Webster (35, 38), and *C. durhamensis* Cornet and Traverse (39), but most closely resemble *C. fragilis* Singh from the Barremian–Aptian of the Congo Basin (40). However, the Spanish and African forms are somewhat smaller than the type specimens of *C. fragilis* (41). *Cycadopites* typically occurs in Mesozoic pollen organs of the Cycadales, Bennettitales, Ginkgoales, Czekanowskiales, Peltaspermales, Pentoxylales, Gnetales (42), and *Sanmiguelia*, a Late Triassic seed plant of uncertain relationships (43).

Of the diverse plant groups that produced *Cycadopites*-type pollen, only ginkgoaleans, and possibly cycads, are present as macrofloral remains throughout the amber-bearing outcrops of the Spanish Albian (32, 44); specimens previously identified as Bennettitales were misinterpreted. In particular, the ginkgoalean foliage genera *Eretmophyllum* [sensu *Nehvizdya* (44–47)] and *Pseudotorellia* are two of the three dominant plants represented (32, 44). It is the more abundant *Eretmophyllum* that was the probable source of the *Cycadopites* pollen vectored by *Gymnopollisthrips*, based on pollen structure and taphonomic and paleoecologic evidence detailed below. Although the sole surviving ginkgoalean species, *Ginkgo biloba*, is obligately wind pollinated (15), this current condition is a poor analog toward inferring pollination modes of diverse Mesozoic ginkgoalean taxa, such as *Eretmophyllum*; wind pollination in recent *G. biloba* consequently is uninformative (15, 48). Many Mesozoic ginkgoaleans produce pollen, in addition to extant *G. biloba* (Table S1), that are greater in length than the grains associated with *Gymnopollisthrips*. These two, albeit subtle, features would provide support for a cycad host hypothesis, consistent with the study by Van Konijnenburg–Van Cittert (49) on older, Jurassic pollen from Yorkshire, United Kingdom.

Only the smaller-sized, elliptic pollen grains from the pollen organs of the Mesozoic cycads, *Androstrobus wonnacotti* Harris, *A. szei* Harris, and *A. balmei* Hill (49, 50) and grains from the pentoxylalean male cone *Sahnia nipaensis* Mittre (51) could be affiliated with the clusters of *Gymnopollisthrips* pollen grains. In most cases, these four, potentially affiliate fossil species are variable in shape, ranging from spherical to elliptic. In addition, the genera *Androstrobus* and *Sahnia* are absent from Spanish Albian amber sites, including Peñacerrada I. Also, our thrips-associated pollen grains are morphologically similar to in situ pollen grains of the Triassic cycad *Delemaya spinulosa*, associated with insect coprolites and suggesting insect pollination (13, 17). Cycads of the Zamiaceae, in particular *Macrozamia lucida* (18) and *M. macdonnellii* (5), are the only extant, insect-pollinated clade with species that have pollen grains similar in size and form to those on *Gymnopollisthrips*. Nevertheless zamiaceous cycads also are absent from Spanish Albian macroremains.

Comparisons between* Gymnopollisthrips *borne and similar pollen. In Table S3, we compared structural features of *Cycadopites* grains borne by *Gymnopollisthrips* with other *Cycadopites* grains from major Mesozoic and extant seed-plant clades (49–55). In Table S2, we measured the lengths and widths of 80 *Cycadopites* grains lodged on the bodies of *Gymnopollisthrips* holotypes (40 from *G. minor* and 40 from *G. maior*) to determine pollen conspecificity and the possible presence of plant–host selectivity by each pollinator species (Fig. 2*B*).

Insects. Description of the holotype (MCNA-10731) of* Gymnopollisthrips minor *gen. et sp. nov. The characteristics of the macropterous female are as follows: body length, 973 μm;. long and short specialized setae with regularly seriate small rings (ring setae) along their length present on the head (anteroventral position), mesopleura, femora, abdomen (lateral and apical positions, almost only on segments IX and X), and wings (distal fringe and distal setae on longitudinal veins).

Head. The characteristics of the head are as follows (measurements are in microns): the head is poorly preserved in the dorsal side (121 long; 152 wide), but an anterior projection of the vertex is present, only one lateral ocellus is preserved, and only four interocellar setae are visible; the ventral side of the head is covered by transverse linear sculpture. The antenna is nine-segmented [total length, 333; segment lengths: segment I, 21; segment II, 45; segment III, 55; segment IV, 52; segment V, 58; segment VI, 55; segment VII, 27; segment VIII, 24; segment IX, 30]; annulae and microtrichia are present on all antennal segments; planate (plate-like) sensory areas in lateroexternal position on segments III (24 long) and IV (28 long), both longitudinally elongated and covering approximately half of the segment length; segment I is short, segment II is asymmetrical with a small prolongation at ventro-lateral apex, and segments II to IX are elongate, cylindrical; segments VI to IX clearly distinct

from each other; segment IX is longer than VIII with *ca.* seven subdivisions. The mouthcone reaches the base of the prosternum; maxillary palps are three-segmented, and labial palps are two-segmented.

Thorax. The characteristics of the thorax are as follows (measurements are in microns): pronotum transverse, 148 long and 194 wide, with the surface finely striate-reticulate; two pairs of long posteroangular setae [76 long (longest)], two pairs of anteroangular setae, and two pairs of lateral setae; only four pairs of posteromarginal setae visible (others being covered). The forewing is not falcate, 676 long and 82 wide at midlength, with microtrichia on membrane; presence of two complete main longitudinal veins, one crossvein between them slightly basal with respect to half of the wing length plus two crossveins at 2/5 of the wing length and other two slightly distal with respect to 3/5 of the wing length, between longitudinal veins and wing margins; longitudinal veins bearing an uninterrupted row of long setae (18 setae in anterior vein and 15–17 in posterior one, up to 48 long). Longitudinal veins ending 55 of wing apex. Anterior margin with a row of setae and a row of short fringe cilia. Posterior fringe straight and not very long (182 the longest). Hindwing narrow, slightly narrowed at apex, not falcate, circa 645 long and 76 wide at midlength, with one slightly sclerotized longitudinal vein closer to the posterior wing margin, reaching the wing apex, with microtrichia on membrane and with fringe not undulate (fringe near the wing apex is 90 long). Mesonotal surface with transverse linear sculpture. All coxae, femora and tibiae with fine transverse sculpture. Foreleg 455 long (femur 182 long and 79 greatest width, tibia 185 long and 39 greatest width, tarsus 58 long and arolium 30 long); forefemur strongly incrassate with a row of dorsal setae; tibia with two stout setae on ventral position [better visible in the paratype (MCNA-9472)]; tarsus (90 long) without a distal hamus. Midlegs are 348 long. Hindleg is 409 long; femur with 2–3 dorsal, large setae; tibia with a row of dorsal setae progressively longer toward distal position and two strong ventrodistal setae. Tarsi are two-segmented.

Abdomen. The characteristics of the abdomen are as follows (measurements are in microns): abdomen with apex slender; pleurites present; abdominal tergites with transverse linear sculpture and sternites with reticulate sculpture. Abdominal tergite X is obscure; trichobothria not observed; strong lateral setae on segments I to VIII; segment IX with two or three pairs of short and strong lateral setae; segment X with four pairs of long and strong setae (specialized ring setae, see diagnosis and below) and about 11 pairs of shorter setae as illustrated (Fig. 1*D*); longest pair, 170 long, is close the basal part of the segment. The ovipositor is upwardly curved, *ca.* 300 long, with margin apparently serrate and bearing a few lateral fine setae.

Description of the holotype (MCNA-9283) of* Gymnopollisthrips maior *sp. nov. For the macropterous female (Fig. S1), the body length is 1,312 μm. Long specialized ring setae with regularly slightly marked rings along their length are present on abdominal segments IX and X; a few ring setae, but shorter, are present on the thorax and hind femur.

Head. Measurements are in microns. The head is quadrangular (142 long; 142 wide); ocellar setae I arise on a conical tubercle (Fig. S3), ocelli are not preserved; interocellar setae are strong (39 long), and three pairs of strong postocular setae are present (about 39 long); the ventral and dorsal sides of the head are covered by transverse linear sculpture. The antenna is nine-segmented (total length, about 380; lengths of segments: II, 48; III, 66; IV, 67; V, 49; VI, 46; VII, 34; VIII, 34; IX, 35); annulae and microtrichia are present on all antennal segments; plate-like sensory areas in lateroexternal position are present on segments III (18 long; 23 wide) (Fig. S2) and IV (24 long, 18 wide); segment I is short, with two strong setae distally; segment II is asymmetrical, with a small prolongation at ventro-lateral apex; segments II to IX are elongate, cylindrical; segments VI to IX are clearly distinct from each other; segment IX has *ca.* seven subdivisions (Fig. S3). The mouthcone reaches the base of the prosternum; maxillary and labial palps are obscure.

Thorax. Measurements are in microns. The pronotum is nearly as long as wide (176 in length; 185 width), with the surface apparently not striate–reticulate; two pairs of long posteroangular setae [85 (longest) and 42 long, respectively], two pairs of anteroangular setae, and four pairs of lateral setae are present; seven pairs of posteromarginal setae are present. The forewing is not falcate (758 long and 118 wide at midlength), with microtrichia on the membrane; two complete main longitudinal veins are present, with one crossvein between them slightly basal with respect to half of the wing length plus two crossveins at two-fifths of the wing length and other two distal with respect to three-fifths of the wing length, between longitudinal veins and wing margins; longitudinal veins bear an uninterrupted row of long setae (about 24 setae on anterior vein and about 21 on posterior one, up to 45 long). Longitudinal veins end 75 of the wing apex. Clavus with a row of five long setae (up to 39 long) and a discal seta is visible on left forewing (30 long). Anterior margin with a row of setae plus a short fringe is present. The posterior fringe is straight and long (288 the longest). The hindwing is narrow, slightly narrowed at apex, not falcate, *ca.* 642 long and 91 wide at midlength, with one slightly sclerotized longitudinal vein closer to the posterior wing margin, reaching the wing apex, with microtrichia on membrane and with long fringe not undulate (182 the longest). Mesonotal surface has transverse linear sculpture. Fine transverse sculpture on legs is only observed on coxae and hind femora. Forefemur is incrassate (about 165 long and 103 greatest wide), with a row of strong dorsal setae (about 15 setae); foretibia (about 175 long) has two stout setae on ventral position; tarsus (90 long) and is without a distal hamus. Midfemur is 39 long, tibia is 160 long, and tarsus is 82 long. The greatest width of hindfemur is 55, and bears with two strong dorsal setae; tibia (252 long) has a row of dorsal setae progressively longer distally and two strong ventrodistal setae; tarsus is 94 long. Tarsi are two-segmented.

Abdomen. The abdomen with apex is slender; pleurites are present; abdominal sternites have transverse linear sculpture; strong lateral setae are present on segments I to VIII; segment IX has three pairs of short and strong lateral setae and two large ventral setae [88 μm (the longest)]; segment X has four pairs of long, strong lateral setae, from which one pair is specialized ring setae (see below), plus *ca.* nine pairs of shorter setae as illustrated (Fig. 2*A*); the longest pair (182 μm long) is close to the basal part of the segment. Tergite X is obscure, and the potential presence of trichobothria is unclear. Ovipositor is upwardly curved, *ca.* 440 long, with margin apparently serrate and bearing a few lateral fine setae.

Other specimens. Apart from the type specimens, described above, an additional female was found with *ca.* 50 pollen grains distributed ventrally, principally on her abdominal terminus. This specimen (MCNA-9516) and an adjacent, additional incomplete specimen, both bearing antennal sensilla and specialized ring setae characteristic of the genus, occur in a small, dark amber piece (Fig. 1*A*), which also contains four males. Because of poor preservation and difficulty of observing characters, these specimens remain identified as *Gymnopollisthrips* sp. Males lack both special setae and attached pollen grains, and despite their bad preservation, they can be identified as males by the presence of prominent abdominal tergal spines. In addition, the amber piece contains a group of *ca.* 70 isolated grains positioned at 2.5 mm from the female individual.

Family-level assignment of the thrips genus. These fossils are attributable to the Aeolothripidae–Melanthripidae–Merothripidae group of families, supported by the synapomorphy "capture of M by RP and the formation of a combined RP+M" (56). The inner phylogeny of this clade remains unresolved, so the apomorphies

that would support assignment to one of the three families are not clearly defined. As indicated in the main text, an attribution to the family Melanthripidae is supported by the presence of a projection in the anterior part of the vertex, with ocellar setae I situated apically, paralleling the melanthripid genus *Ankothrips* (57). *Ankothrips* and *Gymnopollisthrips* also bear an asymmetry of segment II, although in a different conformation (as a ventro-lateral prolongation at the apex). This is however smaller in the fossils than the lobes in extant *Ankothrips*. The sensilla on antennal segments III and IV of fossils are broader than in *Ankothrips* but of about equivalent size to those observed in fossil *Archankothrips varicornis* (58, 59), which possesses the characteristic lobes of *Ankothrips* on the antennal segment II. As in *Ankothrips*, the fossils present stout setae on the apex of the foretibia, a characteristic also observable in *Cranothrips* (60) and *Dorythrips*, whereas in *Melanthrips*, the fourth melanthripid genus, these setae are broad spurs. Other characteristics are congruent with an attribution to Melanthripidae, particularly the broad forewings (also present in Aeolothripidae), the long setae on the pronotum (also present in the merothripid genus *Erotidothrips*), the nine-segmented antenna with segments VI to IX clearly distinct from each other and the antennal segment IX as long as or longer than segment VIII (also present in the aeolothripid genera *Cycadothrips* and *Dactuliothrips*, and in the merothripid genus *Erotidothrips*), the disposition of the setae on antennal segments II and III (which excludes the Aeolothripidae), and broad planate sensilla (this characteristic is also present in some Aeolothripidae and Merothripidae). Nevertheless, the Cretaceous specimens have a set of remarkable characteristics that preclude them to belong to a recent genus. Insufficient preservation of the abdomens in all fossil specimens prevents us to elucidate the presence and morphology of both trichobothria on tergite X and on the lobes of sternite VII, characteristics present in both Melanthripidae and Merothripidae. In conclusion, we attribute these fossils to the family Melanthripidae and await a better resolution of the phylogeny of the three aforementioned families.

We note that the paratype of *Gymnopollisthrips minor* (MCNA-9472) has forewings with 17 setae on the anterior longitudinal vein and about 15 setae on posterior longitudinal vein (vs. 18 and 15–17 in the holotype). These features are best visible in the paratype, rather than the holotype of this species, in which the forefemur is strongly incrassate (227 μm in length; 106 μm in greatest width).

Apart from the diagnostic characteristics discussed in the main text, *G. maior* differs from *G. minor* in having slightly more pronounced linear sculpture on the body, more abundant and robust setae on head and thorax, and two distal crossveins of the forewing that are more distally located.

Ring setae. The torus-like rings that form the distinctive sculpture of the specialized ring setae (Figs. 1 *E–G* and 2 *E–H*) are very conspicuous and present on numerous pairs of setae on diverse external, protruding parts of the body in *G. minor* but less conspicuously so in *G. maior*. Rings of these unique setae considered out of context could be confused with small debris attached to thrips bodies during immersion in resin or regarded as other extraneous artifacts. Features of these setae that indicate that the presence of rings as an anatomical feature characteristic of the genus are: (*i*) ring setae are distributed in a bilateral symmetrical manner on major body regions, such as wings; (*ii*) rings have a regularly spaced occurrence along the length of each seta; (*iii*) rings are fundamentally homogeneous in both shape and size throughout all bearing specimens; (*iv*) ring setae are observed on all female *Gymnopollisthrips* specimens and never have been observed on other insect specimens (including other thrips) in Spanish amber; (*v*) holotype specimens occur in transparent amber and lack particles that could be trapped by the setae during immersion in resin; and (*vi*) isolated or irregularly distributed, ring-like particles have not been observed attached to other setae from the same *Gymnopollisthrips* specimens.

Diverse, special setae in thrips can be related to various activities such as mating, flight, and oviposition, but we infer a function involving collection and transportation of pollen grains. Such a function for ring setae is based on several features: (*i*) ring setae are typically located in the external, protruding parts of the body; (*ii*) rings increase the surface area of each seta, allowing for potential attachment of pollen grains; (*iii*) ring setae have not been observed in thrips specimens that lack attached pollen grains; (*iv*) pollen grains associated with ring setae are always the same palynospecies; (*v*) ring setae are present in all of the female specimens ($n = 4$) of the two species of *Gymnopollisthrips*; and (*vi*) the presence of abundant pollen grains in the basal parts of ring setae and their absence in the distal parts indicate both a direct association between pollen grains and ring setae and relocation of pollen grains by the thrips before flight. The three last circumstances also would be inconsistent with an accidental presence of pollen grains on the bodies of the thrips specimens.

Flight in modern thrips is often preceded by several minutes of abdominal and wing flexing, waving of the forelegs, and wing combing with the legs (61, 62). Such movements may be involved in the relocation of pollen grains to other regions of the body, whereby better transport would be assured. This is a crucial issue, because it has been reported that recent pollinating thrips of cycads lose approximately half of the pollen grains in transport from the time they depart male cones until they alight on female cones (4, 6, 63). It is likely that amber entombment of thrips laden with relocated pollen occurred in flight soon after departure from a pollen organ.

Paleoecology and Taphonomy. Four important amber deposits are known from the Spanish Albian (32, 33), some of which were formerly considered as upper Aptian–lower Albian. The deposits are El Soplao in Cantabria (44, 45), San Just and Arroyo de la Pascueta in Teruel Province (46), and Peñacerrada I in Burgos Province (33, 34). Peñacerrada I is the deposit that contains the amber pieces with the several thrips inclusions that were covered by clusters of pollen grains. These deposits originated in deltaic environments and contain abundant, exceptionally well-preserved plant cuticles.

Plant assemblages from these deposits are dominated by *Frenelopsis*, an arborescent cheirolepidiaceous conifer that produced distinctive, abundant pollen grains of *Classopollis* type. Less abundant are the foliage genera *Eretmophyllum* and *Pseudotorellia*, which produced the rare pollen of *Cycadopites* type. An important observation of some earlier authors is that *Frenelopsis* was one of the amber source plants for the Spanish Lower Cretaceous (45, 64). This inference is buttressed by the presence of *Frenelopsis* axes attached to amber in channel facies from the El Soplao outcrop (32). Najarro, Menor-Salván, and coworkers (45, 64) also have ascertained a cheirolepidiaceous botanical origin for this amber, reinforcing this hypothesis. These authors determined a cheirolepidiaceous source by characterizing specific biomarkers and other diagnostic compounds of *Frenelopsis* foliage, which they compared with known compounds from amber in the same deposit, concluding that they share the same botanical attribution.

Both *Frenelopsis* and *Eretmophyllum* from Spanish Albian amber outcrops show anatomical evidence for xeromorphy (46, 65, 66). It has been proposed that these plants grew along the lower reaches of the delta plain, around ponds and interdistributary bays that record marine and freshwater water input, producing substrates with variable salinity levels (47, 65). Based on analogous data from the Czech Republic, arborescent *Eretmophyllum* was the first unequivocal halophyte among the Ginkgoales. The Czech data strongly support the conclusion that the ginkgoalean *Eret-*

mophyllum occupied water-stressed environments within a coastal salt marsh (65). Altogether, these data suggest that the ginkgoalean taxa grew very close to the resiniferous plants.

The presence of several amber-entombed individuals of the two *Gymnopollisthrips* species that vectored abundant and body-adhering *Cycadopites* pollen grains indicates that the local Peñacerrada I assemblage included resiniferous plants and at least one pollinated gymnosperm. This proposed pollination mutualism involved thrips, miniscule insects that are not particularly efficient in flight, as are very small insects, such as mymarid and mymarommatid wasps with highly reduced wings that lack veins (or are very reduced) and instead bear numerous long fringe setae. This type of flight effectively results in swimming through air as a viscous medium (67) and represents a type of pollination indicating the proximity of *Gymnopollisthrips* to their host plant or plants. *Gymnopollisthrips* and other insect taxa probably arrived at and were entrapped in resin flows soon after their flight from male plant-host organs.

Our examination of the 3D coverage of pollen grains on the *G. minor* holotype (specimen MCNA-10731) supports this inference (Movie S1). The *G. minor* specimen is covered by *ca.* 140 pollen grains on the thorax and distal abdomen (Fig. 1 *B–D*). Adjacent to this thrips, 1 mm distant, is a small, internal amber surface covered by *ca.* 150 pollen grains (Fig. 2 *I* and *J*). Another isolated cluster containing about 70 grains occurs in the amber piece bearing specimen MCNA-9516 at 2.5 mm from this female thrips with pollen loads (*ca.* 50 pollen grains) (Fig. 1*A*). The paratype specimen of *G. minor* bears only *ca.* 15 pollen grains on the ventral part of the abdomen and an additional few grains on the dorsal aspect. The holotype specimen of *G. maior* contains *ca.* 137 pollen grains in contact with its thoracic ventral surface, but some of them are detached and form an attenuated tail (Fig. 2*A* and Fig. S1). This phenomenon has been observed in Cenozoic ambers with other obligate pollinators (68), such as bees and fig wasps that possess structures for pollen grain attachment (68, 69). For the Peñacerrada I thrips, several grains, often in clusters, contact the basal parts of the long ring setae of the distal abdomen and ventral wing surfaces (Figs. 1 *H–J* and 2 *E–H*). The four thrips carrying pollen grains are females; parallel observations show that modern female *Cycadothrips* pollinate *Macrozamia* cycads and transport a notably higher quantity of pollen grains than males (6). These distributions of clustered and isolated grains of monospecific pollen in amber may be explained by the plant hosts simultaneously possessing both insect and wind types of pollination (ambophily), occurring in a few extant species of cycads (2, 70).

An important aspect of fossil thrips pollination inferred from amber inclusions and associated macrofossils is the parautochthonous nature of Spanish Albian deposits, indicating that ginkgoalean and cycad plants could have been the source of the *Cycadopites* pollen. In addition to the ecological conditions required by the cheirolepidiaceous *Frenelopsis* and ginkgoalean *Eretmophyllum*, at El Soplao, there are *Frenelopsis* vegetative shoots that are commonly branched up to four ranks, suggesting parautochthonous deposition (45). Additionally, both abscised leaves and ovulate reproductive organs of *Eretmophyllum*, assigned to the form-genus *Nehvizdyella*, were hydrodynamically transported together despite their different shape, indicating the absence of long distance transport. Alternatively, the most similar pollen grains to *Cycadopites* pollen occurring on *Gymnopollisthrips* are those found in situ for an Antarctic Triassic cycad species (13) and the pollen grains of some extant species of *Macrozamia* cycads pollinated by *Cycadothrips* (5, 6, 63). Thus, some palynological data suggest that cycads may have been pollinated by Cretaceous thrips. Cycads at Peñacerrada I may have inhabited the forest understory, perhaps growing among *Frenelopsis* plants and producing few vegetative remains of low fossilization potential, explaining their rarity in cuticle assemblages.

Palynological examination of the amber-bearing sediments from the Peñacerrada I deposit also indicates the rare presence of monosulcate pollen grains, typically cited as *Monosulcites* sp. (71), which similarly are scarce in other Albian amber outcrops throughout Spain (45, 72, 73). This parallel pattern of comparatively rare monosulcate grain distribution would be similar to that of *Cycadopites*, if insects were pollinating a source plant of relatively short stature and producing low levels of pollen within the understory of dense forests. This situation is found in modern thrips pollinators of short-statured, frequently herbaceous angiosperms (Table S3). Regional vegetation based on palynological studies reveal that everwet, mixed conifer forests existed on more elevated alluvial plains, whereas xeromorphic vegetation that included short-statured plants were adapted to coastal environments, as represented by cheirolepidiaceous conifers, ferns adapted to dry conditions, gnetaleans, and other seed plants with psilate and monosulcate pollen grains such as ginkgoaleans and cycads (74).

In conclusion, megafossil and taphonomic data strongly suggest an association of *Gymnopollisthrips* with *Eretmophyllum*. By contrast, palynological evidence is more indicative of a *Gymnopollisthrips*–cycad association, allowing for a viable hypothesis of an association with cycads.

Fossil Taxa for Phylogeny Calibration. The references of the thrips taxa listed in the legend of Fig. 3 for Thysanoptera phylogeny are as follows: *Cyphoneurodes patriciae* (75) (Fig. 3, numbered 1); *Burmacypha longicornis* (76) (Fig. 3, numbered 2); *Triassothrips virginicus* (77) (Fig. 3, numbered 3); *Kazachothrips triassicus* (78) (Fig. 3, numbered 4); *Karataothrips jurassicus* (79) (Fig. 3, numbered 5); *Cretothrips antiquus* (77) (Fig. 3, numbered 6); extant *Cycadothrips chadwicki* (6) (Fig. 3, numbered 7); *Gymnopollisthrips minor*, *G. maior* (this report) (Fig. 3, numbered 8); *Tethysthrips libanicus* (80) (Fig. 3, numbered 9); *Tethysthrips hispanicus* (80) (Fig. 3, numbered 10); several extant genera (Table S3) (Fig. 3, numbered 11); several occurrences in Lebanese amber (81) (Fig. 3, numbered 12); *Hispanothrips utrillensis* (82) (Fig. 3, numbered 13); and *Rohrthrips libanicus* (80) (Fig. 3, numbered 14). The Lophioneuridae are indicated as a sister-group of the Thysanoptera. Represented plant groups have geological age ranges taken from Taylor et al. (83); the superimposed thysanopteran phylogeny is mainly from two publications (84, 85), with limited modification. The thysanopteran phylogeny is calibrated by a geochronology (86).

1. Schneider D, Wink M, Sporer F, Lounibos P (2002) Cycads: Their evolution, toxins, herbivores and insect pollinators. *Naturwissenschaften* 89:281–294.
2. Kono M, Tobe H (2007) Is *Cycas revoluta* (Cycadaceae) wind- or insect-pollinated? *Am J Bot* 94:847–855.
3. Terry I, Walter GH, Moore C, Roemer R, Hull C (2007) Odor-mediated push-pull pollination in cycads. *Science* 318:70.
4. Niklas KJ, Buchmann SL, Kerchner V (1986) Aerodynamics of *Ephedra trifurca*. I. Pollen grain velocity fields around stems bearing ovules. *Am J Bot* 73:966–979.
5. Mound LA, Terry I (2001) Thrips pollination of the Central Australian cycad, *Macrozamia macdonnellii* (Cycadales). *Int J Plant Sci* 162:147–154.
6. Terry I (2001) Thrips and weevils as dual, specialist pollinators of the Australian cycad *Macrozamia communis* (Zamiaceae). *Int J Plant Sci* 162:1293–1305.
7. Terry I (2002) *Thrips and Tospoviruses: Proceedings of the Seventh International Symposium on Thysanoptera*, eds Marullo R, Mound LA (Australian National Insect Collection, Canberra, Australia), pp 157–162.
8. Terry I, et al. (2009) Cone insects and putative pollen vectors of the endangered cycad, *Cycas micronesica*. *Micronesica* 41:83–99.
9. Crowson RH (1991) *Advances in Coleopterology*, eds Zunino M, Belles X, Blas M (European Association of Coleopterology, Barcelona), pp 13–28.
10. Chavez R, Genaro JA (2005) A new species of *Pharaxonotha* (Coleoptera: Erotylidae), probable pollinator of the endangered Cuban cycad, *Microcycas calocoma* (Zamiaceae). *Insecta Mundi* 19:143–150.
11. Jolivet P (2005) Cycads and beetles: Recent views on pollination. *Cycad Newslett* 28: 3–7.

12. Tang W (2004) *Vistas in Paleobotany and Plant Morphology: Evolutionary and Environmental Perspectives*, ed Srivastava PC (UP Offset, Lucknow, India), Prof. D. D. Pant Memorial Volume, pp 383–394.
13. Klavins SD, Kellogg DW, Krings M, Taylor EL, Taylor TN (2005) Coprolites in a Middle Triassic cycad pollen cone: Evidence for insect pollination in early cycads? *Evol Ecol Res* 7:479–488.
14. Wang J, Labandeira CC, Zhang G, Bek J, Pfefferkorn HW (2009) Permian *Circulipuncturites discinisporis* Labandeira, Wang, Zhang, Bek et Pfefferkorn gen. et spec. nov. (formerly *Discinispora*) from China, an ichnotaxon of a punch-and-sucking insect on Noeggerathialean spores. *Rev Palaeobot Palynol* 156:277–282.
15. Labandeira CC, Kvaček J, Mostovski MB (2007) Pollination drops, pollen, and insect pollination of Mesozoic gymnosperms. *Taxon* 56:663–695.
16. Ren D, et al. (2009) A probable pollination mode before angiosperms: Eurasian, long-proboscid scorpionflies. *Science* 326:840–847.
17. Labandeira CC (2010) The pollination of Mid Mesozoic seed plants and the early history of long-proboscid insects. *Ann Mo Bot Gard* 97:469–513.
18. Dehgan B, Dehgan NB (1988) Comparative pollen morphology and taxonomic affinities in Cycadales. *Am J Bot* 75:1501–1516.
19. Osborn JM, Taylor TN (1995) Pollen morphology and ultrastructure of the Bennettitales: In situ pollen of *Cycadeoidea. Am J Bot* 82:1074–1081.
20. Labandeira CC (2005) *The Evolutionary Biology of Flies*, eds Yeates DK, Wiegmann BM (Columbia Univ Press, New York), pp 217–272.
21. Norstog KJ, Stevenson DW, Niklas KJ (1986) The role of beetles in pollination of *Zamia furfuracea. Biotropica* 18:300–306.
22. Kato M, Inoue T (1994) Origin of insect pollination. *Nature* 368:195.
23. Meeuse ADJ, De Meijer AH, Mohr OWP, Wellinga SM (1990) Entomophily in the dioecious gymnosperm *Ephedra aphylla* Forsk. (=*E. alte* C.A. Mey.), with some notes on *Ephedra campylopoda* C.A. Mey. III: Further anthecological studies and relative importance of entomophily. *Isr J Bot* 39:113–123.
24. Tafforeau P, et al. (2006) Applications of X-ray synchrotron microtomography for non-destructive 3D studies of paleontological specimens. *Appl Phys, A Mater Sci Process* 83:195–202.
25. Lak M, et al. (2008) Phase contrast X-ray synchrotron imaging: Opening access to fossil inclusions in opaque amber. *Microsc Microanal* 14:251–259.
26. Soriano C, et al. (2010) Synchrotron X-ray imaging of inclusions in amber. *C R Palevol* 9:361–368.
27. Paganin D, Mayo SC, Gureyev TE, Miller PR, Wilkins SW (2002) Simultaneous phase and amplitude extraction from a single defocused image of a homogeneous object. *J Microsc* 206:33–40.
28. Friis EM, et al. (2007) Phase-contrast X-ray microtomography links Cretaceous seeds with Gnetales and Bennettitales. *Nature* 450:549–552.
29. Martin T, et al. (2009) LSO-based single crystal film scintillator for synchrotron-based hard X–ray micro–imaging. *IEEE Trans Nucl Sci* 56:1412–1418.
30. Labiche JC, et al. (2007) The fast readout low noise camera as a versatile x-ray detector for time resolved dispersive extended x-ray absorption fine structure and diffraction studies of dynamic problems in materials science, chemistry, and catalysis. *Rev Sci Instrum* 78:091301.
31. Martínez–Torres LM, Pujalte V, Robles S (2003) Los yacimientos de ámbar del Cretácico Inferior de Peñacerrada (Álava, Cuenca Vasco–Cantábrica): Estratigrafía, reconstrucción paleogeográfica y estructura tectónica. *Est Mus Cienc Nat Álava* 18:9–32.
32. Peñalver E, Delclòs X (2010) *Biodiversity of Fossils in Amber from the Major World Deposits*, ed Penney D (Siri Scientific Press, Manchester), pp 236–270.
33. Delclòs X, et al. (2007) Fossiliferous amber deposits from the Cretaceous (Albian) of Spain. *C R Palevol* 6:135–149.
34. Alonso J, et al. (2000) A new fossil resin with biological inclusions in Lower Cretaceous deposits from Álava (northern Spain, Basque–Cantabrian Basin). *J Paleontol* 74:158–178.
35. Fensome RA (1983) Miospores from the Jurassic–Cretaceous Boundary Beds, Aklavik Range, Northwest Territories, Canada; Incorporating taxonomic reviews of several groups of Mid- to Late Mesozoic miospores. Thesis (Univ of Saskatchewan, Saskatoon, Canada).
36. Wodehouse RP (1933) Tertiary pollen II. The oil shales of the Eocene Green River Formation. *Bull Torrey Bot Club* 60:479–524.
37. Wilson LR, Webster RM (1946) Plant microfossils from a Fort Union coal of Montana. *Am J Bot* 33:271–278.
38. Filatoff J (1975) Jurassic palynology of the Perth Basin, Western Australia. *Palaeontographica B* 154:1–113.
39. Cornet B, Traverse A (1975) Palynological contributions to the chronology and stratigraphy of the Hartford Basin in Connecticut and Massachusetts. *Geosci Man* 11:1–33.
40. Dejax J (1987) Une étude palynologique dans le Crétacé Inférieur du Congo. Thesis (Université Pierre et Marie Curie, Paris, France).
41. Singh C (1964) Microflora of the Lower Cretaceous Mannville Group, East–Central Alberta. *Res Counc Alberta Bull* 15:1–239.
42. Balme BE (1995) Fossil in–situ spores and pollen grains: An annotated catalogue. *Rev Palaeobot Palynol* 87:81–323.
43. Cornet B (1986) The leaf venation and reproductive structures of a Late Triassic angiosperm, *Sanmiguelia lewisii. Evol Theory* 7:231–301.
44. Najarro M, et al. (2009) Unusual concentration of Early Albian arthropod-bearing amber in the Basque–Cantabrian Basin (El Soplao, Cantabria, Northern Spain). *Geol Acta* 7:363–387.
45. Najarro M, et al. (2010) Review of the El Soplao amber outcrop, Early Cretaceous of Cantabria, Spain. *Acta Geol Sin* 84:959–976.
46. Gomez B, Barale G, Martín–Closas C, Thévenard F, Philippe M (1999) Découverte d'une flore à Ginkgoales, Bennettitales et Coniférales dans le Crétacé inférieur de la Formation Escucha (Chaîne Ibérique Orientale, Teruel, Espagne). *Neues Jb Geol Paläont Mh* 1999:661–675.
47. Gomez B, Martín-Closas C, Barale G, Thévenard F (2000) A new species of *Nehvizdya* (Ginkgoales) from the Lower Cretaceous of the Iberian Ranges (Spain). *Rev Palaeobot Palynol* 111:49–70.
48. Nel A (1997) The probabilistic inference of unknown data in phylogenetic analysis. *Mém Mus Natl Hist Nat* 173:305–327.
49. Van Konijnenburg-Van Cittert JHA (1971) In situ gymnosperm pollen from the Middle Jurassic of Yorkshire. *Acta Bot Neerl* 20:1–97.
50. Hill CR (1990) Ultrastructure of in situ fossil cycad pollen from the English Jurassic, with a description of the male cone *Androstrobus balmei* sp. nov. *Rev Palaeobot Palynol* 65:165–173.
51. Suthar OP, Sharma BD (1988) A new interpretation on the structure of *Sahnia nipaniensis* Mittre from the Rajmahal Hills. *Palaeobotanist* 37:90–93.
52. Liu X-Q, Li C-S, Wang Y-F (2006) The pollen cones of *Ginkgo* from the Early Cretaceous of China, and the bearing on the evolutionary significance. *Bot J Linn Soc* 152: 133–144.
53. Krassilov VA, Bugdaeva EV (1988) Gnetalean plants from the Jurassic of Ust–Balej, east Siberia. *Rev Palaeobot Palynol* 53:359–374.
54. Townrow JA (1960) The Peltaspermaceae, a pteridosperm family of Permian and Triassic age. *Palaeontology* 3:333–361.
55. Osborn JM, Taylor TN, Crane PR (1991) The ultrastructure of *Sahnia* pollen (Pentoxylales). *Am J Bot* 78:1560–1569.
56. Nel P, et al. (2012) From Carboniferous to Recent: Wing venation enlightens evolution of thysanopteran lineage. *J Syst Palaeontol*, in press.
57. Bagnall RS (1926) Fossil Thysanoptera. IV. Melanothripidae. *Entomol Mon Mag* 60: 16–17.
58. Mound LA (1968) A review of R.S. Bagnall's Thysanoptera collections. *Bull Br Mus Nat Hist (Entomol)* (Suppl 11):3–181.
59. Bailey SF (1940) A review of the genus *Ankothrips* D.L. Crawford. *Pan-Pac Entomol* 16: 97–106.
60. Pereyra V, Mound LA (2009) Phylogenetic relationships within the genus *Cranothrips* (Thysanoptera, Melanthripidae) with consideration of host associations and disjunct distributions within the family. *Syst Entomol* 34:151–161.
61. Lewis T (1973) *Thrips, Their Biology, Ecology and Economic Importance* (Academic Press, New York).
62. Ellington CP (1980) Wing mechanics and take-off preparation of thrips (Thysanoptera). *J Exp Biol* 85:129–136.
63. Terry I, et al. (2005) Pollination of Australian *Macrozamia* cycads (Zamiaceae): Effectiveness and behavior of specialist vectors in a dependent mutualism. *Am J Bot* 92:931–940.
64. Menor-Salván C, et al. (2010) Terpenoids in extracts of Lower Cretaceous ambers from the Basque–Cantabrian Basin (El Soplao, Cantabria, Spain): Paleochemotaxonomic aspects. *Org Geochem* 41:1089–1103.
65. Kvaček J, Falcon-Lang HJ, Dašková J (2005) A new Late Cretaceous ginkgoalean reproductive structure *Nehvizdyella* gen. nov. from the Czech Republic and its whole-plant reconstruction. *Am J Bot* 92:1958–1969.
66. Gomez B, et al. (2002) *Frenelopsis* (Coniferales: Cheirolepidiaceae) and related male organ genera from the Lower Cretaceous of Spain. *Palaeontology* 45:997–1036.
67. Grodnitsky DL (1995) Evolution and classification of insect flight kinematics. *Evolution* 49:1158–1162.
68. Peñalver E, Engel M, Grimaldi DA (2006) Fig wasps in Dominican amber (Hymenoptera: Agaonidae). *Am Mus Novit* 3541:1–16.
69. Weiblen GD (2002) How to be a fig wasp. *Annu Rev Entomol* 47:299–330.
70. Procheş Ş, Johnson SD (2009) Beetle pollination of the fruit-scented cones of the South African cycad *Stangeria eriopus*. *Am J Bot* 96:1722–1730.
71. Barrón E, Comas-Rengifo MJ, Elorza L (2001) Contribuciones al estudio palinológico del Cretácico Inferior de la Cuenca Vasco–Cantábrica: Los afloramientos ambarígenos de Peñacerrada (España). *Col Paleontol* 52:135–156.
72. Peyrot D, Rodríguez-López JP, Lassaletta L, Meléndez N, Barrón E (2007) Contributions to the palaeoenvironmental knowledge of the Escucha Formation in the Lower Cretaceous Oliete Sub-basin, Teruel, Spain. *C R Palevol* 6:469–481.
73. Solé de Porta N, Querol X, Cabanes R, Salas R (1994) Nuevas aportaciones a la palinología y paleoclimatología de la Formación Escucha (Albiense inferior-medio) en las cubetas de Utrillas y Oliete, Cordillera Ibérica Oriental. *Cuad Geol Ibérica* 18: 203–215.
74. Diéguez C, Peyrot D, Barrón E (2010) Floristic and vegetational changes in the Iberian Peninsula during Jurassic and Cretaceous. *Rev Palaeobot Palynol* 162:325–340.
75. Beckemeyer RJ, Hall JD (2007) The entomofauna of the Lower Permian insect beds of Kansas and Oklahoma, USA. *Afr Invertebr* 48:23–39.
76. Zherikhin VV (2000) A new genus and species of Lophioneuridae from Burmese amber (Thripida (=Thysanoptera): Lophioneurina). *Bull Nat Hist Mus Lond* 56:39–41.
77. Grimaldi DA, Shmakov A, Fraser N (2004) Mesozoic thrips and early evolution of the order Thysanoptera (Insecta). *J Paleontol* 78:941–952.
78. Shmakov AS (2008) The Jurassic thrips *Liassothrips crassipes* (Martynov, 1927) and its taxonomic position in the order Thysanoptera (Insecta). *Paleontol. J* 42:47–52.
79. Sharov AG (1972) The phylogenetic relations of the order Thysanoptera. *Entomol Obozr* 51:854–858.
80. Nel P, Peñalver E, Azar D, Hodebert G, Nel A (2010) Modern thrips families Thripidae and Phlaeothripidae in Early Cretaceous amber (Insecta: Thysanoptera). *Ann Soc Entomol Fr* 46:154–163.
81. zur Strassen R (1973) Insektenfossilien aus der unteren Kreide. 5. Fossile Fransenflügler aus mesozoischem Bernstein des Libanon (Insecta: Thysanoptera). *Stuttg Beitr Naturkd, A* 256:1–51.
82. Peñalver E, Nel P (2010) *Hispanothrips* from Early Cretaceous Spanish amber, and a new genus of the resurrected family Stenurothripidae (Insecta: Thysanoptera). *Ann Soc Entomol Fr* 46:138–147.

83. Taylor TN, Taylor EL, Krings M (2009) *Paleobotany: The Biology and Evolution of Fossil Plants* (Academic Press, New York).
84. Heming BS (1993) *Functional Morphology of Insect Feeding*, eds Schaefer CS, Leschen RAB (Thomas Say Publ. Entomol, Lanham, MD), pp 3–41.
85. Mound LA, Heming BS, Palmer JM (1980) Phylogenetic relationships between the families of recent Thysanoptera (Insecta). *Zool J Linn Soc* 69:111–141.
86. Ogg JG, Ogg G, Gradstein FM (2008) *The Concise Geologic Time Scale* (Cambridge Univ Press, Cambridge, UK).

Fig. S1. Habitus of *Gymnopollisthrips maior* sp. nov. Microphotographs of the holotype in lateral (*Upper*) and ventral (*Lower*). Views are at the same scale.

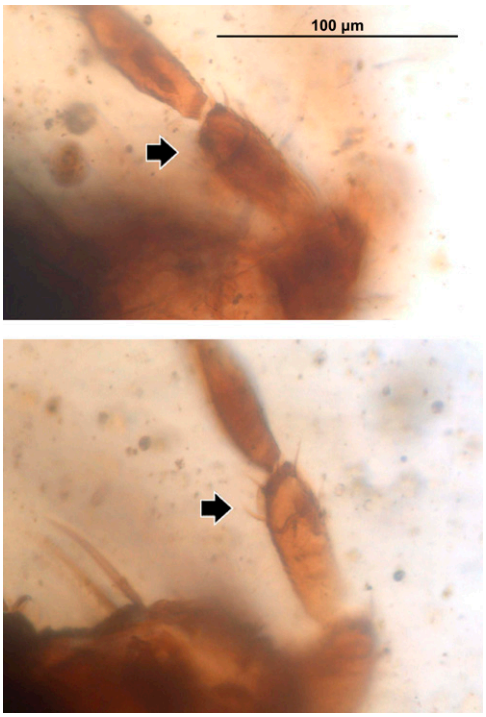

Fig. S2. Planate sensory structure on antennal segment III of *Gymnopollisthrips maior* sp. nov. Microphotographs in lateral view of the planated sensory structure (arrows) on segment III of both antennae from the holotype, at same scale.

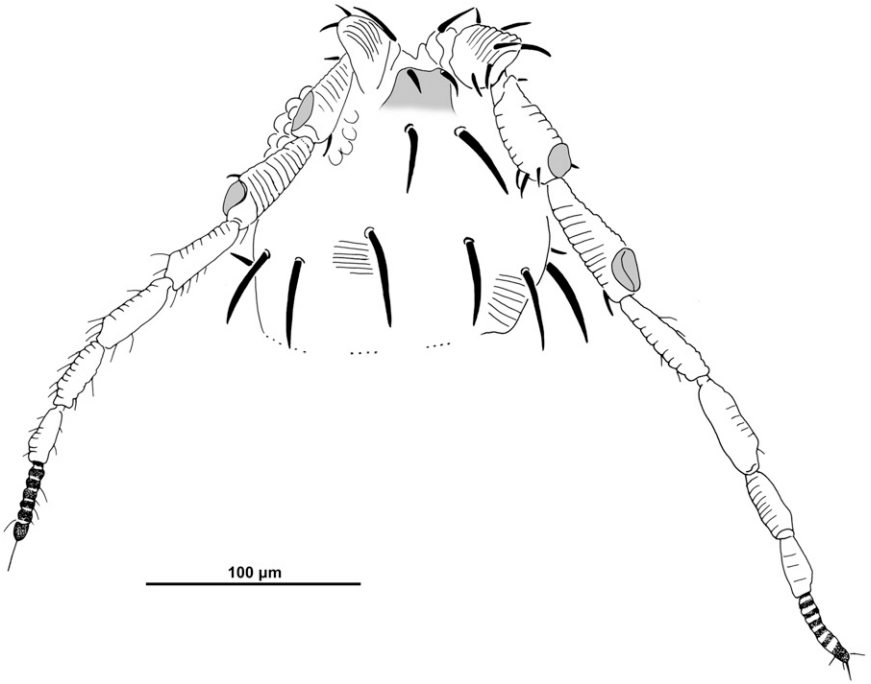

Fig. S3. Head of *Gymnopollisthrips maior* sp. nov. Camera lucida drawing of the head in dorsal view. Plate-like sensory areas and conical tubercle with ocellar setae I are colored in gray.

Table S1. Ability of modern thrips to carry pollen

Plant host taxon	Thrips pollinator taxon	No. of thrips examined	Greatest no. of grains observed	Average grains per thrips	Source
Fossil gymnosperms					
Gymnosperm indet. (Ginkgoales or Cycadales)	*Gymnopollisthrips minor* gen. et sp. nov. (Melanthripidae)	2	140	77.5	This report
Gymnosperm indet. (Ginkgoales or Cycadales)	*Gymnopollisthrips maior* sp. nov. (Melanthripidae)	1	137	137	This report
Extant gymnosperms*					
Macrozamia macdonnellii (Zamiaceae)	*Cycadothrips albrechti* (Aeolothripidae)	38 (10)	69 (24)	20.5 (15.1)	1
Macrozamia communis (Zamiaceae)	*Cycadothrips chadwicki* (Aeolothripidae)	66 (56)	255 (96)	52.1 (21.6)	2
Macrozamia lucida (Zamiaceae)	*Cycadothrips chadwicki* (Aeolothripidae)	531 (258)	223 (145)	107 (29.2)	3
Extant angiosperms†					
Medicago sativa (Fabaceae)	*Frankliniella tritici* (Thripidae)	130	16	2.3	4
Eschscholzia californica (Papaveraceae)	*Frankliniella tritici* (Thripidae)	96	20	3.3	4
Bellis perennis (Asteraceae)	*Frankliniella minuta* (Thripidae)	20	4	2.0	4
Prunus domestica (Rosaceae)	*Frankliniella tritici* (Thripidae)	16	3	0.2	4
Eschscholzia californica (Papaveraceae)	*Anaphothrips secticornis* (Thripidae)	10	3	3	4
Beta vulgaris (Chenopodiaceae)	*Thrips tabaci* (Thripidae)	2	140	137	4
Castilla elastica (Moraceae)	*Frankliniella diversa* (Thripidae)	1,099	72	7.6–25.8	5
Shorea lepidota (Dipterocarpaceae)	*Thrips* sp. (Thripidae)	70	27	2.43	6
Chloranthus serratus (Chloranthaceae)	*Taeniothrips eucharii* (Thripidae)	2	>40	38	7
Macaranga hullettii (Euphorbiaceae)	*Neoheegeria* sp. (Phlaeothripidae)	91	268	63.6	8

*Counts include thrips departing male cones and no. of thrips subsequently arriving at female cones.
†Representative examples for comparison, not an exhaustive list from the bibliography.

1. Mound LA, Terry I (2001) Thrips pollination of the Central Australian cycad, *Macrozamia macdonnellii* (Cycadales). *Int J Plant Sci* 162:147–154.
2. Terry I (2001) Thrips and weevils as dual, specialist pollinators of the Australian cycad *Macrozamia communis* (Zamiaceae). *Int J Plant Sci* 162:1293–1305.
3. Terry LI, et al. (2005) Pollination of Australian *Macrozamia* cycads (Zamiaceae): Effectiveness and behavior of specialist vectors in a dependent mutualism. *Am J Bot* 92:931–940.
4. Lewis T (1973) *Thrips, Their Biology, Ecology and Economic Importance* (Academic Press, New York).
5. Sakai S (2001) Thrips pollination of androdioecious *Castilla elastica* (Moraceae) in a seasonal tropical forest. *Am J Bot* 88:1527–1534.
6. Appanah S, Chan HT (1981) Thrips: The pollinators of some dipterocarps. *Malaysian Forester* 44:234–252.
7. Luo Y, Li Z (1999) Pollination ecology of *Chloranthus serratus* (Thunb.) Roem. et Schult. and *Ch. fortunei* (A. Gray) Solms–Laub. (Chloranthaceae). *Ann Bot (Lond)* 83:489–499.
8. Moog U, Fiala B, Federle W, Maschwitz U (2002) Thrips pollination of the dioecious ant plant *Macaranga hullettii* (Euphorbiaceae) in Southeast Asia. *Am J Bot* 89:50–59.

Table S2. Length and width measurements of pollen grains on *Gymnopollisthrips* holotypes

Gymnopollisthrips minor (MCNA-10731)		*Gymnopollisthrips maior* (MCNA-9283)	
Length (μm)	Width (μm)	Length (μm)	Width (μm)
22.6	10.8	23.5	11.7
21.0	12.5	21.2	11.7
19.3	12.4	19.2	13.3
19.7	9.7	19.9	16.2
22.1	10.4	23.8	14.0
18.6	13.8	22.1	12.9
21.5	9.3	22.1	11.9
21.0	13.7	22.3	14.4
17.7	10.4	21.5	12.5
19.9	12.2	19.2	11.5
18.8	13.6	20.0	10.2
20.2	14.4	20.0	13.1
19.2	11.5	20.0	11.5
19.7	11.6	16.5	9.4
20.6	11.3	20.1	13.5
21.4	12.1	18.4	11.9
19.7	12.3	20.0	13.6
20.0	9.9	20.6	14.2
23.5	12.8	17.4	10.8
22.5	11.2	18.8	12.9
21.1	10.6	19.9	12.5
23.0	12.5	21.9	12.8
21.8	11.6	22.7	14.6
24.9	13.1	19.9	13.3
21.1	14.1	20.2	11.7
21.2	12.4	21.2	9.6
21.0	12.8	21.1	11.3
20.0	12.1	20.0	14.3
19.2	12.2	19.8	15.4
20.6	13.4	19.8	11.5
22.4	11.3	17.7	18.1
19.7	14.1	21.1	13.5
19.2	11.9	18.6	13.9
23.2	10.9	16.7	13.9
19.0	11.7	15.3	13.4
18.6	11.7	18.8	12.4
19.9	15.8	21.6	14.0
22.1	11.3	20.1	11.4
21.5	11.9	21.8	12.6
21.2	15.4	19.3	11.5

Table S3. Morphology of in situ *Cycadopites* pollen from fossil and extant gymnosperms

Order	Taxon	Length (μm)	Width (μm)	Exine (μm)	Age	Shape	Source
On *Gymnopollisthrips minor* and *G. maior*							
Ginkgoales or Cycadales	Indet. (*Cycadopites* pollen form genus)	20.4 (17.4–24.9)	12.6 (9.3–15.4)	1.3 (0.7–2.5)	Lower Albian	Elliptic	This study
Modern taxa							
Cycadales	*Bowenia spectabilis* Hook ex. Hook	30.32 ± 1.01	18.70 ± 0.98		Extant		18
Cycadales	*Cycas revoluta* Thunb.	27.5–34.3	34.2–23.8	4.8–7.2	Extant	Almost spherical	Our data
Cycadales	*Dioon edule* Lindl.	28.32 ± 0.96	22.00 ± 1.18		Extant		18
Cycadales	*Encephalartos ferox* (G. Bertol.) Lehm.	32.72 ± 1.35	19.78 ± 0.31		Extant		18
Cycadales	*Lepidozamia peroffskyana* Regel	38.40 ± 1.82	20.18 ± 1.12		Extant		18
Cycadales	*Macrozamia lucida*	21.57 ± 1.24	11.13 ± 1.09		Extant	Elliptic	18
L.A.S. Johnson							
Cycadales	*Macrozamia macdonnellii* (Miq.) A. DC.	~25	~13		Extant		5
Cycadales	*Macrozamia miquelii* (F. Muell.) A. DC.	24.18 ± 1.53	11.07 ± 0.69		Extant		18
Ginkgoales	*Ginkgo biloba* L.	24.9–35.9	16.9–28.9	3.0–5.4	Extant	Elliptic to spherical	Our data
Fossil taxa							
Bennettitales	*Cycadeoidea dacotensis* Macbride	~25	~12	~0.73	Lower Cretaceous	Ovoid to spherical	19
Bennettitales	*Williamsoniella coronata* Thomas	22–33		0.5–1	Middle Jurassic	Elliptic to almost circular	49
Cycadales	*Androstrobus balmei* Hill	20.5–29.0	14.5–19.8	0.57–1.16	Middle Jurassic	Ovoid	50
Cycadales	*Androstrobus szei* Harris [light microscopy]	24–32		1–1.5	Middle Jurassic	Elliptic to almost spherical	49
Cycadales	*Androstrobus szei* Harris [S.E.M.]	24.5–31	14.5–19.5	>0.56	Middle Jurassic	Ovoid to broadly ovoid	50
Cycadales	*Androstrobus wonnacotti* Harris [light microscopy]	24–33		1.5–2	Middle Jurassic	Elliptic to circular	49
Cycadales	*Androstrobus wonnacotti* Harris [S.E.M.]	20–25	15–19	0.45–0.65	Middle Jurassic	Broadly ovoid to subspherical	50
Cycadales	*Delemaya spinulosa* Klavins et al.	~20	~13		Middle Triassic	Broadly ovoid (ellipsoidal)	13
Ginkgoales	*Ginkgo huttoni* (Sternberg) Heer	29–42		1–1.5	Middle Jurassic	Elongated–elliptic	49
Ginkgoales	*Ginkgo liaoningensis* Liu, Li & Wang	31	>13		Lower Cretaceous	Elongated–elliptic	52
Ginkgoales	*Nehvizdyella bipartita* Kvaček, Falcon–Lang & Dašková	26.3–30.8	14.7–25.6		Upper Cretaceous	Boat-shaped	64
Gnetales	*Aegianthus sibiricum* (Heer) Krassilov	30–42.5	20–26	1.5	Middle Jurassic	Elliptic; ornamented with pits	53
Peltaspermales	*Antevsia extans* (Frenguelli) Townrow	23–35	13–23		Lower and Middle Triassic	Spindle-shaped	54
Peltaspermales	*Antevsia zeilleri* (Nathorst) Harris	29–46.25	20–29.8		Upper Triassic	Spindle-shaped	54
Pentoxylales	*Sahnia laxiphora* Drinnan & Chambers	24–28	20–25		Lower Cretaceous	Ovoid	55
Pentoxylales	*Sahnia nipaensis* Mittre	10–22	7–17		Jurassic	Elliptic or circular	51
Incertae sedis	*Synangispadixis tidwellii* Cornet	21–29	11–19		Upper Triassic	Elliptic; tectate–granular	43

S.E.M., scanning electron microscopy.

Movie S1. Three-dimensional movie of the holotype specimen of *Gymnopollisthrips minor* gen. et sp. nov. (MCNA-10731) imaged by synchrotron tomography to better study the pollen distribution. All of the pollen grains detected by synchrotron tomography have been colored in yellow.

Movie S1